Article

Cooperation of σ–π and σ*–π* Conjugation in the UV/Vis and Fluorescence Spectra of 9,10-Disilylanthracene

Soichiro Kyushin * and **Yuya Suzuki**

Division of Molecular Science, Graduate School of Science and Technology, Gunma University,
Kiryu 376-8515, Gunma, Japan; osicl-0903@yahoo.co.jp
* Correspondence: kyushin@gunma-u.ac.jp

Abstract: In 1996, we reported that silyl groups of 9,10-disilylanthracenes significantly affect the UV/Vis and fluorescence spectra. Although the results indicate that the silyl groups have strong electronic effects on anthracene, the details of the mechanisms responsible for this have not yet been clarified. This article describes the analysis of the UV/Vis and fluorescence spectra of 9,10-bis(diisopropylsilyl)anthracene by theoretical calculations. This study reveals that π conjugation of anthracene is extended by cooperation of σ–π and σ*–π* conjugation between the silyl groups and anthracene. This effect increases the transition moment of the π–π* transition of anthracene. As a result, the molecular extinction coefficient of the ^1L_a band and the fluorescence quantum yield are increased.

Keywords: anthracene; fluorescence spectrum; σ–π conjugation; σ*–π* conjugation; silyl group; UV/Vis spectrum

1. Introduction

Studies on the electronic effects of silyl groups go back to the middle of the last century. The electronic effects of silyl groups were recognized by unusual accelerations of the reactions of some organosilicon compounds [1]. Later, the electronic effects were observed by UV [2] and photoelectron [3] spectroscopies. Today, σ–π conjugation between σ(Si–C or Si–Si) and π orbitals [4], σ*–π* conjugation between σ*(Si–C) and π* orbitals [5] are well known. These electronic effects are considered to be caused by relatively high energy levels of the σ orbitals, relatively low energy levels of the σ* orbitals and large lobes of the σ and σ* orbitals.

In 1996, we reported that silyl groups of 9,10-bis(diisopropylsilyl)anthracene (**1**, Figure 1) and related 9,10-disilylanthracenes significantly affect the UV/Vis and fluorescence spectra [6]. The absorption maximum of the ^1L_a band in the UV/Vis spectrum of **1** (λ_{max} = 399 nm (ε = 14200 mol^{-1} L cm^{-1})) shows a considerable bathochromic shift with the large molecular extinction coefficient compared with that of anthracene (λ_{max} = 374 nm (ε = 8000 mol^{-1} L cm^{-1})). The fluorescence quantum yield of **1** (Φ_f = 0.90 (room temperature)) is much larger than that of anthracene (Φ_f = 0.32 (room temperature)). These results indicate that the silyl groups affect both the HOMO and LUMO. Similar results have also been reported by other groups [7–10]. After this finding, UV/Vis, fluorescence and other measurements of various silyl-substituted aromatic compounds have been reported, showing electronic effects of silyl groups [11–29].

In spite of numerous studies on the UV/Vis and fluorescence spectra of silyl-substituted aromatic compounds, the effects of silyl groups have not yet been fully determined. On the other hand, studies on the UV/Vis spectra of unsubstituted aromatic compounds have been fruitful in recent years [30]. Studies on the substituent effects of silyl groups are important not only for the development of fundamental organosilicon chemistry, but also from the viewpoint of optoelectronic applications to dyes and luminescent materials. We report

herein a theoretical analysis of the electronic effects of the silyl groups of **1** at the TD-DFT B3LYP/6-31G(d) level. We found that cooperation of electronic effects of the silyl groups in the HOMO and LUMO is important in the UV/Vis and fluorescence spectra of **1**.
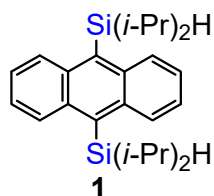
Figure 1. Structure of **1**.

2. Results and Discussion

2.1. Measurement of the UV/Vis and Fluorescence Spectra of **1** and Anthracene

In our previous paper [6], we compared the ^1L_a band of **1** at 300–450 nm with that of anthracene [31–34]. To get a big picture, the whole UV/Vis spectra of **1** and anthracene were measured (Figure 2). The intense absorption band at ca. 250 nm and the vibration bands at 300–380 nm of anthracene had already been assigned to the ^1B and ^1L_a bands, respectively [35–37]. The UV/Vis spectrum of **1** has three features: (1) The molecular extinction coefficient of the ^1B band (λ_{max} = 262 nm (ε = 102,000 mol^{-1} L cm^{-1})) is much smaller than that of anthracene (λ_{max} = 252 nm (ε = 190,000 mol^{-1} L cm^{-1})); (2) On the other hand, the molecular extinction coefficient of the ^1L_a band (λ_{max} = 400 nm (ε = 14,000 mol^{-1} L cm^{-1})) is larger than that of anthracene (λ_{max} = 375 nm (ε = 7200 mol^{-1} L cm^{-1})); and (3) The ^1B and ^1L_a bands of **1** show bathochromic shifts compared with those of anthracene.
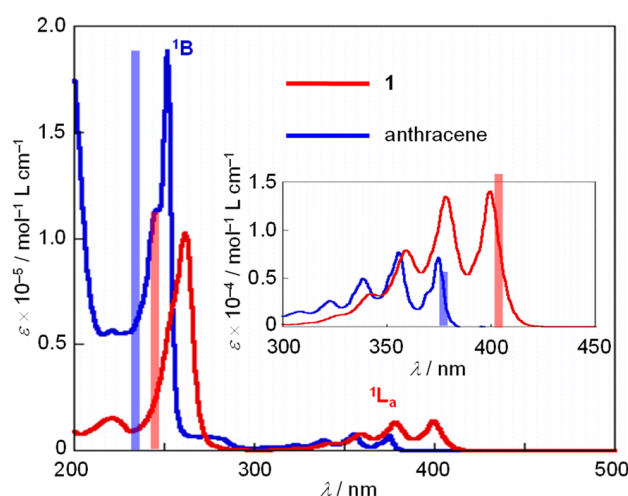
Figure 2. UV/Vis spectra of **1** and anthracene in hexane at room temperature. The pale red (**1**) and blue (anthracene) bars denote absorption calculated by using the optimized structures of the S_0 states of **1** and anthracene at the TD-DFT B3LYP/6-31G(d) level.

We also measured the fluorescence spectra of **1** and anthracene at 77 K (Figure 3). The fluorescence of anthracene is observed at 370–520 nm, whereas the fluorescence bands of **1** shift bathochromically to 400–570 nm. These fluorescence spectra resemble those measured at room temperature [6], although the vibrational fine structures are sharp, and peaks are more separated. The fluorescence quantum yield of **1** (Φ_f = 0.98 (77 K)) is much larger than that of anthracene (Φ_f = 0.34 (77 K)) [38]. The phosphorescence of **1** and anthracene could not be observed. The phosphorescence quantum yield of anthracene has been reported to be very small (Φ_p = 0.0003 [38]). The data of the UV/Vis and fluorescence spectra of **1** and anthracene are summarized in Table 1.
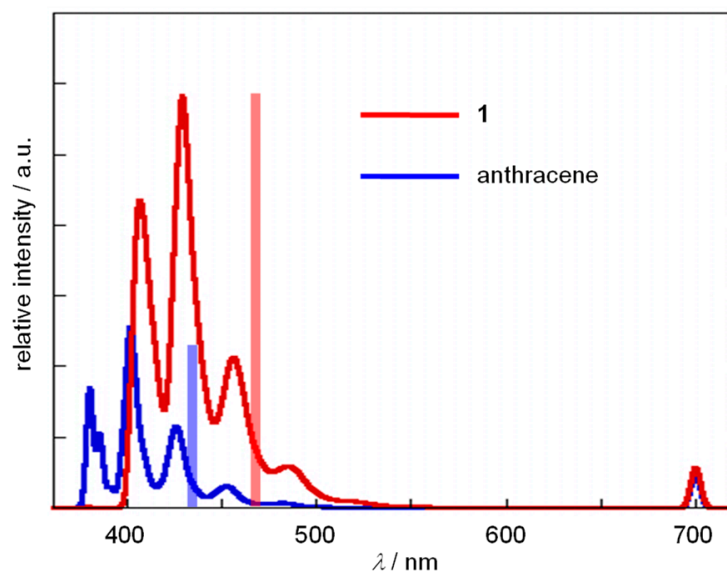
Figure 3. Fluorescence spectra of **1** and anthracene in 3-methylpentane at 77 K. The pale red (**1**) and blue (anthracene) bars denote fluorescence calculated by using the optimized structures of the S_1 states of **1** and anthracene at the TD-DFT B3LYP/6-31G(d) level.

Table 1. Photophysical parameters of **1** and anthracene.

Compound	λ_a/nm [1] (ε/mol^{-1} L cm^{-1})	λ_f/nm [2]
1	221 (15,400) 262 (102,000) 343 (3400) 359 (7900) 378 (13,500) 400 (14,000)	406 429 456 485
anthracene	252 (190,000) 323 (2700) 339 (5000) 356 (7700) 375 (7200)	380 402 426 453 482

[1] Measured in hexane at room temperature. [2] Measured in 3-methylpentane at 77 K.

2.2. Theoretical Analysis of the UV/Vis Spectra of **1** and Anthracene

The HOMO, HOMO–1, LUMO and LUMO+1 of **1** and anthracene are shown in Figure 4. The energy levels of the HOMO and HOMO–1 of **1** are similar to those of anthracene. However, the HOMO of **1** clearly shows out-of-phase interaction between σ(Si–C) orbitals and a π orbital of the anthracene moiety (σ–π conjugation, Figure S1) [11,15,16,25,28]. The effect of the σ–π conjugation on the energy levels is small probably because the distance between the σ(Si–C) and π orbitals is relatively large. The energy levels of the LUMO and LUMO+1 of **1** are lower than those of anthracene. Notably, the LUMO clearly shows in-phase interaction between the σ*(Si–C) and π* orbitals of anthracene (σ*–π* conjugation, Figure S1) [5,15,16,25,28]. The relatively small distance between the σ*(Si–C) and π* orbitals makes the energy level of the LUMO low. TD-DFT calculations show that the ^1L_a bands of **1** and anthracene are mainly due to the HOMO-to-LUMO transitions with the configuration-interaction (CI) coefficient of 0.70 (Table S3). The energy gaps between the HOMO and LUMO are 3.40 (**1**) and 3.59 eV (anthracene). The smaller energy gap of **1** is in accordance with the bathochromic shift of the ^1L_a band compared with that of anthracene.
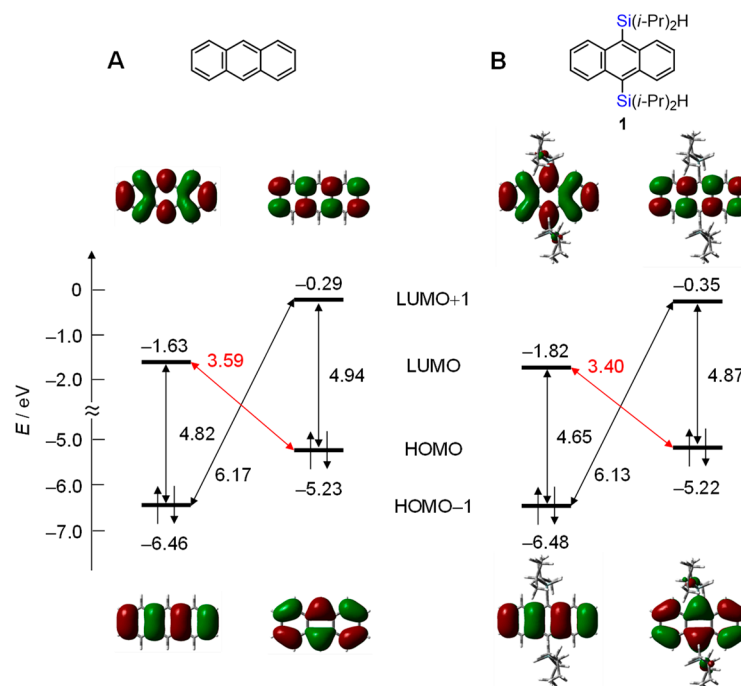
Figure 4. The HOMO, HOMO–1, LUMO, LUMO+1 and their energy levels of **1** (**B**) and anthracene (**A**) calculated at the B3LYP/6-31G(d) level.

The transition moments of the HOMO-to-LUMO transitions of **1** and anthracene are 1.46 and 0.85 a.u., respectively. The large transition moment of **1** corresponds to the large molecular extinction coefficient of the ^1L_a band of **1** (Figure 2) [6]. As the HOMO-to-LUMO transition mainly contributes to the ^1L_a band, the transition moment can be expressed by

$$\mu \approx \int \psi_{HOMO} \boldsymbol{M} \psi_{LUMO} \, d\tau \tag{1}$$

where ψ_{HOMO} and ψ_{LUMO} are the wave functions of the HOMO and LUMO, respectively. $\boldsymbol{M}$ is the operator of the dipole moment [39–42]. The multiplication of ψ_{HOMO} and ψ_{LUMO} is shown in Scheme 1. The σ–π and σ*–π* conjugation give positive (or negative) areas just outside of the positive (or negative) areas of the π orbital of the anthracene ring. This extension of areas with the same signal occurs at the 9,10-positions of anthracene. As the transition moment of anthracene is in the direction of the short molecular axis, this extension increases the transition moment. Therefore, cooperation of the σ–π and σ*–π* conjugation makes the molecular extinction coefficient of the ^1L_a band of **1** larger than that of anthracene.
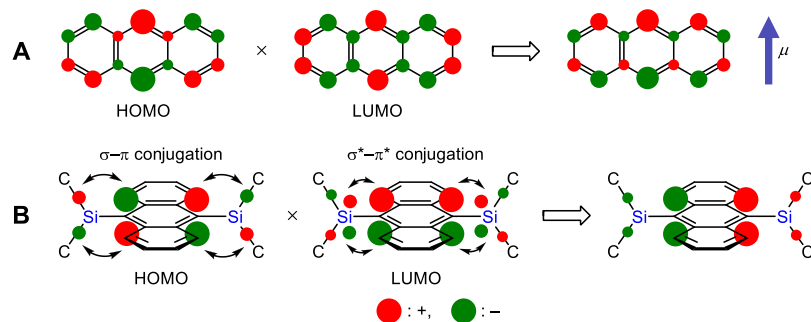
Scheme 1. Multiplication of the HOMO and LUMO of anthracene and the transition moment of the HOMO–LUMO transition (**A**). The effect of the silyl groups on the transition moment is shown in the (**B**).

The TD-DFT calculation showed that the ^{1}B band of anthracene is formed by the CI between the HOMO–1-to-LUMO and HOMO-to-LUMO+1 transitions; other transitions do not contribute to this band (Figure 5A). Both transitions have transition moments in the direction of the long molecular axis of anthracene. These two transition moments are enhanced by each other, as shown by the CI coefficients, giving the large total transition moment of 3.83 a.u. Similarly, the ^{1}B band of **1** is formed by the CI between the HOMO–1-to-LUMO and HOMO-to-LUMO+1 transitions (Figure 5B). Although the transition moments of these transitions are enhanced by each other, the total transition moment (3.03 a.u.) is significantly smaller than that of anthracene. The squares of the transition moments as well as the oscillator strengths of the ^{1}B bands of **1** ($\mu^2 = 9.2$ a.u.^{2}, $f = 1.14$) and anthracene ($\mu^2 = 14.7$ a.u.^{2}, $f = 1.91$) are nearly in line with the molecular extinction coefficients of the ^{1}B bands (**1**: $\varepsilon = 102000$ mol^{-1} L cm^{-1}, anthracene: $\varepsilon = 190000$ mol^{-1} L cm^{-1}). These results indicate that the difference of the intensity of the ^{1}B bands could be ascribed mainly to the electron transition, although the effect of vibronic coupling could not be completely excluded.
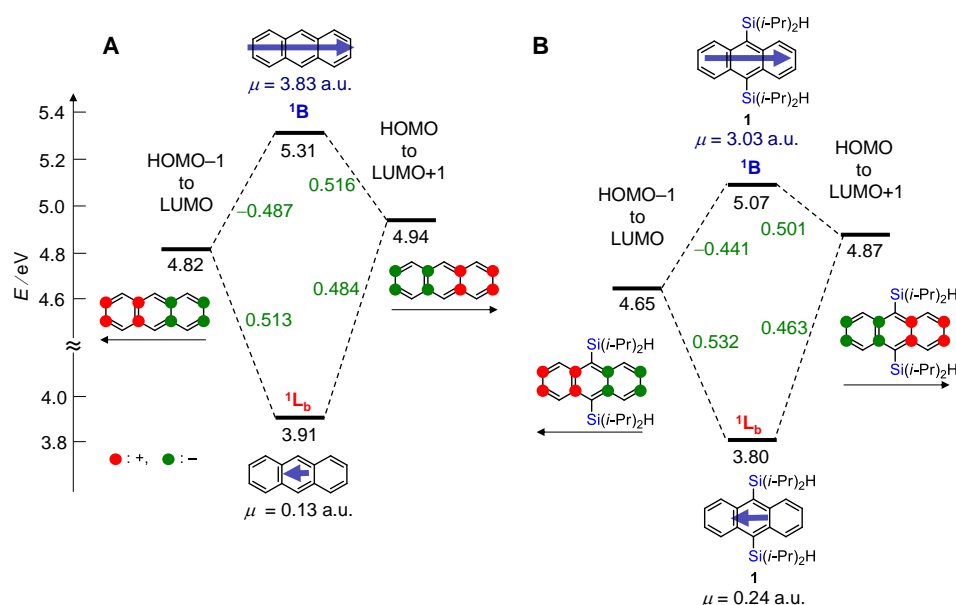
Figure 5. Configuration interaction between transitions for the ^{1}B and ^{1}L$_b$ bands of **1** (**B**) and anthracene (**A**) calculated at the TD-DFT B3LYP/6-31G(d) level. Energy levels were calculated at the B3LYP/6-31G(d) level. The structures with positive and negative circles show the products of orbital pairs representing the transition. The arrows under the structures denote transition moments.

The relatively small transition moment of the ^{1}B band of **1** compared with that of anthracene is ascribed to contribution of the HOMO-to-LUMO+3 transition (Figure 6A,B and Table S3). The CI coefficients of the ^{1}B band of anthracene are −0.487 (HOMO–1-to-LUMO) and 0.516 (HOMO-to-LUMO+1), whereas those of **1** are smaller, i.e.,: −0.441 (HOMO–1-to-LUMO) and 0.501 (HOMO-to-LUMO+1). Instead, the HOMO-to-LUMO+3 transition contributes with the CI coefficient of 0.186. The HOMO-to-LUMO+3 transition of anthracene has a high energy (6.47 eV) and does not interact with the HOMO–1-to-LUMO (4.82 eV) and HOMO-to-LUMO+1 (4.94 eV) transitions. However, the energy level of the LUMO+3 of **1** is very low because of effective σ*–π* conjugation between σ*(Si–C) orbitals and a π* orbital of anthracene (Figure 6). As a result, the HOMO-to-LUMO+3 transition of **1** has a small energy (5.57 eV) and interacts with the HOMO–1-to-LUMO (4.65 eV) and HOMO-to-LUMO+1 (4.87 eV) transitions. The HOMO-to-LUMO+3 transition does not have a transition moment in the direction of the long molecular axis (Figure 6 (bottom)). The relatively reduced contribution of the HOMO–1-to-LUMO and HOMO-to-LUMO+1 transitions to the ^{1}B band leads to the relatively small transition moment.
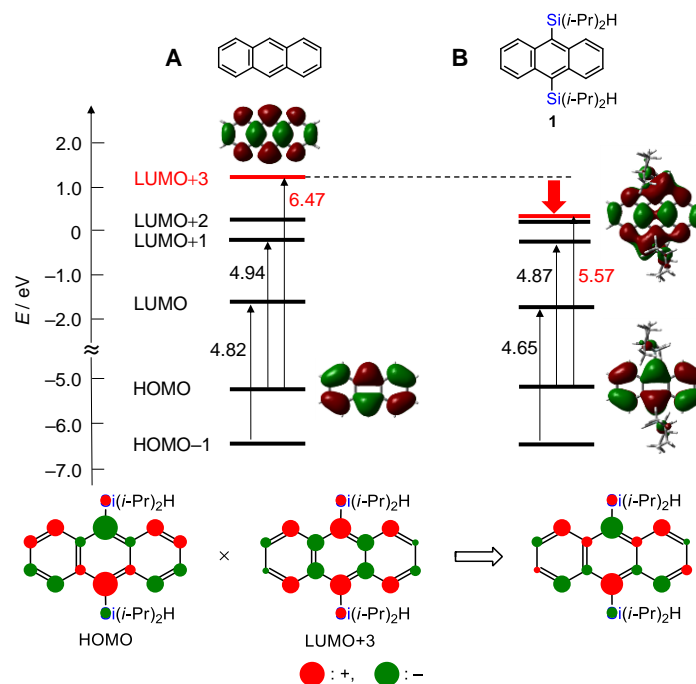
Figure 6. Comparison of the HOMO-to-LUMO+3 transitions of **1** (**B**) and anthracene (**A**) calculated at the B3LYP/6-31G(d) level. The product of the HOMO and LUMO+3 of **1** is shown at the **bottom**.

The discussion of the ^1L_a and ^1B bands shows that the silyl groups affect these bands in different manners. In the ^1L_a band, the silyl groups "directly" enhance the transition moment of anthracene. On the other hand, the silyl groups allow another transition to contribute to the ^1B band. This effect reduces contribution of the original transitions of anthracene and weakens the transition moment. This is an "indirect" effect of the silyl groups.

The TD-DFT calculations also show that the ^1L_b bands of **1** and anthracene must be present at 326 and 317 nm, respectively. However, as the transition moments (**1**: 0.24 a.u., anthracene: 0.13 a.u.) are much smaller than those of the ^1L_a bands (**1**: 1.46 a.u., anthracene: 0.85 a.u.), the ^1L_b bands are hidden by the ^1L_a bands in both compounds.

2.3. Optimized Structures of the Excited Singlet States of **1** and Anthracene

The optimized structures of the excited singlet states (S_1) of **1** and anthracene were calculated at the TD-DFT B3LYP/6-31G(d) level and compared with those of the ground states (S_0). The structures and structural parameters are shown in Figure 7. The S_0 and S_1 states of anthracene have completely planar structures with the D_{2h} symmetry. The anthracene moiety of the S_0 state of **1** has a slightly bent structure with a fold angle (4.7°) between the C9–C9a–C1–C2–C3–C4–C4a–C10 and C10–C10a–C5–C6–C7–C8–C8a–C9 planes. The fold angle increases in the case of the S_1 state (12.6°). The bent structure of the S_1 state of **1** could be explained by the effects of molecular orbitals and steric hindrance. By excitation from the S_0 state to the S_1 state, an electron in the HOMO is transferred to the LUMO. The p orbitals at the 9,10-positions, which have the largest coefficients in the HOMO, interact with the adjacent p orbitals with the in-phase mode (Figure 4). In contrast, the p orbitals at the 9,10-positions in the LUMO interact with the adjacent p orbitals in the out-of-phase mode. The π interaction between the 9,10- and adjacent carbon atoms is weakened by the excitation. In addition, the steric hindrance between the bulky diisopropylsilyl groups and the four hydrogen atoms at the *peri*-positions is present in the planar structure. A combination of these electronic and steric effects results in the bent structure of the anthracene moiety.
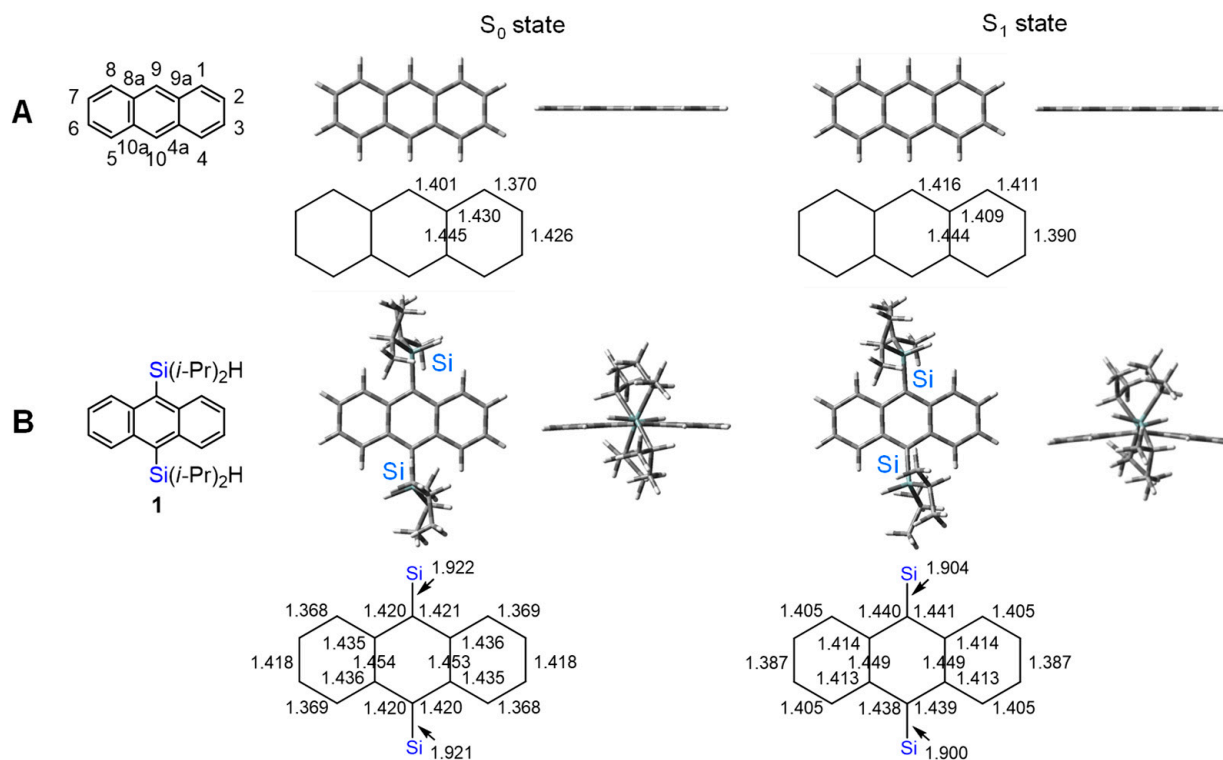
Figure 7. Top and side views and bond lengths (Å) of the optimized structures of the S_0 and S_1 states of **1** (**B**) and anthracene (**A**). The structures of the S_0 and S_1 states were calculated at the B3LYP/6-31G(d) and TD-DFT B3LYP/6-31G(d) levels, respectively.

The optimized structure of the S_1 state of **1** has another feature. The C(1)–C(2), C(3)–C(4), C(5)–C(6) and C(7)–C(8) bonds (1.405 Å) and the C(9)–C(9a), C(4a)–C(10), C(10)–C(10a) and C(8a)–C(9) bonds (1.438–1.441 Å) are longer than the corresponding bonds (1.368–1.369 Å and 1.420–1.421 Å, respectively) of the S_0 state, whereas the C(2)–C(3) and C(6)–C(7) bonds (1.387 Å) and the C(1)–C(9a), C(4)–C(4a), C(5)–C(10a) and C(8)–C(8a) bonds (1.413–1.414 Å) of the S_1 state are shorter than the corresponding bonds (1.418 Å and 1.435–1.436 Å, respectively) of the S_0 state. These structural changes are due to the electron transition from the bonding (or antibonding) π orbital of the HOMO to the antibonding (or bonding) π* orbital of the LUMO. Furthermore, the Si–C(9) (1.904 Å) and Si–C(10) (1.900 Å) bonds of the S_1 state of **1** are shortened compared with the corresponding bonds (1.922 and 1.921 Å, respectively) of the S_0 state. The shortening could be explained by σ*–π* conjugation between the silicon and C(9 or 10) atoms in the LUMO.

*2.4. Theoretical Analysis of the Fluorescence Spectra of **1** and Anthracene*

The S_1 states of **1** and anthracene emit fluorescence and are deactivated to the S_0 states according to the Franck–Condon principle [43,44]. The frontier orbitals and energy levels of the S_1 states of **1** and anthracene calculated by using the optimized S_1 structures are shown in Figure 8. Although the energy level of the HOMO of **1** is similar to that of anthracene, lobes of the HOMO show σ–π conjugation (Figure S2). The energy level of the LUMO of **1** is lower than that of anthracene due to σ*–π* conjugation. The energy gap between the HOMO and the LUMO of the S_1 state of **1** (2.90 eV) is smaller than that of anthracene (3.11 eV). This result is in accord with the bathochromic shift of the fluorescence bands of **1** compared with those of anthracene (Figure 3).
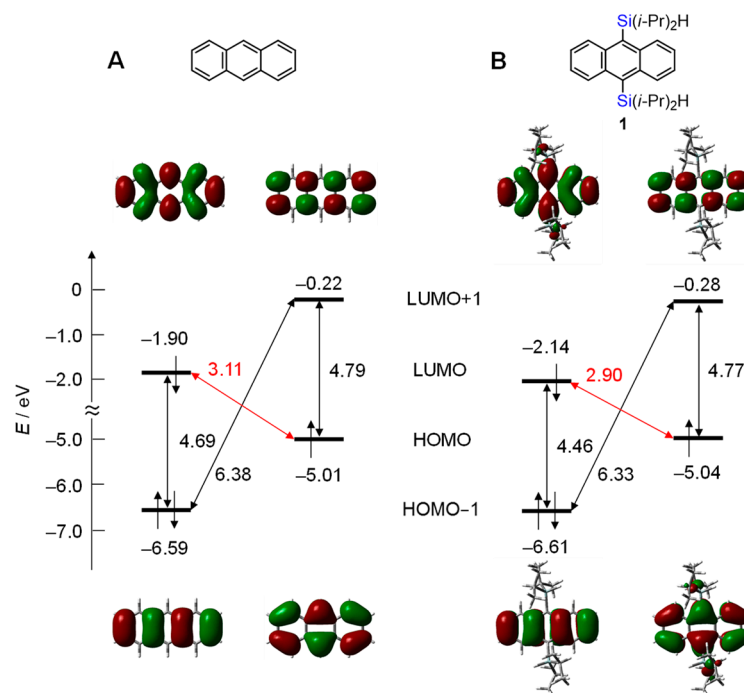
Figure 8. The HOMO, HOMO−1, LUMO, LUMO+1 and their energy levels of the S_1 states of **1** (**B**) and anthracene (**A**) calculated at the B3LYP/6-31G(d) level.

The transition moment of the electron transition from the LUMO to the HOMO of the S_1 state was calculated. The transition moment of **1** (1.55 a.u.) is larger than that of anthracene (0.93 a.u.) by cooperation of σ–π and σ*–π* conjugation, similar to the UV/Vis spectra (Scheme 1, Figure S2). The squares of the transition moments of **1** (μ^2 = 2.42 a.u.^{2}) and anthracene (μ^2 = 0.86 a.u.^{2}) are nearly proportional to the fluorescence quantum yield of **1** (Φ_f = 0.90) and anthracene (Φ_f = 0.32) [6]. It is noted that the transition moment of **1** is larger than that of the electron transition from the HOMO to the LUMO of the S_0 state of **1** (1.46 a.u.). The larger transition moment of the S_1 state is ascribed to the shortening of the Si–C bonds. The short Si–C bonds lead to effective σ–π and σ*–π* conjugation, as shown by larger lobes of the σ(Si–C) and σ*(Si–C) orbitals than those of the S_0 state (Figures S1 and S2). As the lobes of the σ(Si–C) and σ*(Si–C) orbitals become larger, the transition moment becomes larger, as shown in Scheme 1.

3. Materials and Methods

Compound **1** was prepared according to the reported procedure [6]. Anthracene (Merck, Darmstadt, Germany, 99.5%) was purchased and used without further purification.

UV/Vis spectra were recorded on a V-570 UV/VIS/NIR spectrophotometer (JASCO, Hachioji, Japan). Fluorescence spectra were obtained on an F-4500 fluorescence spectrophotometer (Hitachi, Tokyo, Japan). Fluorescence quantum yields were determined by using a C9920-02 absolute PL quantum yield measurement system (Hamamatsu Photonics, Hamamatsu, Japan).

All theoretical calculations were performed by using Gaussian 09 [45] and 16 [46] on a PRIMERGY RX300 system (Fujitsu, Tokyo, Japan) of the Research Center for Computational Science, Japan. The structures of the S_0 and S_1 states of **1** and anthracene were optimized at the B3LYP/6-31G(d) and TD-DFT B3LYP/6-31G(d) levels, respectively, and the optimization was confirmed by frequency calculations. The results are summarized in Tables S1 and S2. Transition properties of **1** and anthracene were calculated at the TD-DFT B3LYP/6-31G(d) level by using the optimized structures. The results are summarized in Tables S3 and S4.

4. Conclusions

This study reveals substituent effects of the silyl groups on the UV/Vis and fluorescence spectra of **1**. Cooperation of the σ–π conjugation in the HOMO and the σ*–π* conjugation in the LUMO leads to the bathochromic shifts of the UV/Vis and fluorescence bands. Furthermore, the decrease of the ^{1}B band, the increase of the ^{1}L$_a$ band, and the increase of the fluorescence quantum yield are rationalized. This is the first step toward clarifying the substituent effects of silyl groups on the optical properties of silyl-substituted aromatic compounds. To develop this work, further studies on the effects of silyl groups at various substitution positions of aromatic compounds and the effects of substituents on a silyl group are necessary. These studies will be undertaken in the near future.

References

1. Jarvie, A.W.P. Anomalous properties of *β*-functional organosilicon compounds—*β*-effect. *Organomet. Chem. Rev. A* **1970**, *6*, 153–207.
2. Sakurai, H.; Kumada, M. The ultraviolet spectra of some polysilanes. *Bull. Chem. Soc. Jpn.* **1964**, *37*, 1894–1895. [CrossRef]
3. Bock, H.; Solouki, B. Photoelectron spectra of silicon compounds. In *The Chemistry of Organic Silicon Compounds*; Patai, S., Rappoport, Z., Eds.; Wiley: Chichester, UK, 1989; pp. 555–653.
4. Traylor, T.G.; Hanstein, W.; Berwin, H.J.; Clinton, N.A.; Brown, R.S. Vertical stabilization of cations by neighboring σ bonds. General considerations. *J. Am. Chem. Soc.* **1971**, *93*, 5715–5725. [CrossRef]
5. Yamaguchi, S.; Tamao, K. Theoretical study of the electronic structure of 2,2′-bisilole in comparison with 1,1′-bi-1,3-cyclopentadiene: σ*–π* conjugation and a low-lying LUMO as the origin of the unusual optical properties of 3,3′,4,4′-tetraphenyl-2,2′-bisilole. *Bull. Chem. Soc. Jpn.* **1996**, *69*, 2327–2334. [CrossRef]
6. Kyushin, S.; Ikarugi, M.; Goto, M.; Hiratsuka, H.; Matsumoto, H. Synthesis and electronic properties of 9,10-disilylanthracenes. *Organometallics* **1996**, *15*, 1067–1070. [CrossRef]
7. Fang, M.-C.; Watanabe, A.; Matsuda, M. Synthesis of σ–π conjugated organosilicon copolymers and their optical properties. *Jpn. J. Appl. Phys.* **1995**, *34* (Suppl. 1), 98–100. [CrossRef]
8. Suzuki, H.; Satoh, S.; Kimata, Y.; Kuriyama, A. Synthesis and properties of poly(methylphenylsilane) containing anthracene units. *Chem. Lett.* **1995**, *24*, 451–452. [CrossRef]
9. Fang, M.-C.; Watanabe, A.; Matsuda, M. Emission spectra of *σ*–π-conjugated organosilicon copolymers consisting of alternating dimethylsilylene and aromatic units. *Macromolecules* **1996**, *29*, 6807–6813. [CrossRef]
10. Satoh, S.; Suzuki, H.; Kimata, Y.; Kuriyama, A. Optical and electroluminescence properties of poly(methylphenylsilane) containing an anthracene unit. *Synth. Met.* **1996**, *79*, 97–102. [CrossRef]

11. Kyushin, S.; Kitahara, T.; Matsumoto, H. Benzo[1,2:4,5]bis(1,1,2,2-tetraisopropyldisilacyclobutene). *Chem. Lett.* **1998**, *27*, 471–472. [CrossRef]

12. Maeda, H.; Inoue, Y.; Ishida, H.; Mizuno, K. UV absorption and fluorescence properties of pyrene derivatives having trimethylsilyl, trimethylgermyl, and trimethylstannyl groups. *Chem. Lett.* **2001**, *30*, 1224–1225. [CrossRef]

13. Kyushin, S.; Takemasa, N.; Matsumoto, H.; Horiuchi, H.; Hiratsuka, H. 2,3,6,7,10,11-Hexakis(dimethylsilyl)triphenylene. *Chem. Lett.* **2003**, *32*, 1048–1049. [CrossRef]

14. Kyushin, S.; Ishikita, Y.; Matsumoto, H.; Horiuchi, H.; Hiratsuka, H. Yellow-green fluorescence of 5,11- and 5,12-bis(diisopropylsilyl)naphthacenes. *Chem. Lett.* **2006**, *35*, 64–65. [CrossRef]

15. Kyushin, S.; Matsuura, T.; Matsumoto, H. 2,3,4,5-Tetrakis(dimethylsilyl)thiophene: The first 2,3,4,5-tetrasilylthiophene. *Organometallics* **2006**, *25*, 2761–2765. [CrossRef]

16. Shimizu, M.; Oda, K.; Bando, T.; Hiyama, T. Preparation, structure, and properties of tris(trimethylsilyl)silyl-substituted anthracenes: Realization of ideal conformation for σ–π conjugation involving eclipse of Si–Si σ-bond with p-orbital of aromatic ring. *Chem. Lett.* **2006**, *35*, 1022–1023. [CrossRef]

17. Karatsu, T. Photochemistry and photophysics of organomonosilane and oligosilanes: Updating their studies on conformation and intramolecular interactions. *J. Photochem. Photobiol. C Photochem. Rev.* **2008**, *9*, 111–137. [CrossRef]

18. Kyushin, S.; Yoshimura, K.; Sato, K.; Matsumoto, H. Hyperchromic effect of silyl groups on the UV–visible spectrum of 5,10,15,20-tetraphenylporphyrin. *Chem. Lett.* **2009**, *38*, 324–325. [CrossRef]

19. Otsuka, K.; Ishida, S.; Kyushin, S. A light-emitting liquid crystal containing *p*-terphenyl and an alkylsilyl group. *Chem. Lett.* **2012**, *41*, 307–309. [CrossRef]

20. Maeda, H.; Maeda, T.; Mizuno, K. Absorption and fluorescence spectroscopic properties of 1- and 1,4-silyl-substituted naphthalene derivatives. *Molecules* **2012**, *17*, 5108–5125. [CrossRef]

21. Toma, Y.; Kuribara, T.; Iizuka, T.; Nagashima, H.; Kyushin, S. Synthesis, structure, and electronic properties of benzohexasilabicyclo[2.2.2]octene. *Chem. Lett.* **2013**, *42*, 250–252. [CrossRef]

22. Horiuchi, H.; Hosaka, M.; Mashio, H.; Terata, M.; Ishida, S.; Kyushin, S.; Okutsu, T.; Takeuchi, T.; Hiratsuka, H. Silylation improves the photodynamic activity of tetraphenylporphyrin derivatives in vitro and in vivo. *Chem. Eur. J.* **2014**, *20*, 6054–6060. [CrossRef] [PubMed]

23. Kyushin, S.; Saito, Y.; Yoshimura, K.; Horiuchi, H.; Hiratsuka, H. Synthesis and properties of 5,10,15,20-tetrakis(4′-trimethylsilylphenyl)chlorin. *Heteroatom Chem.* **2014**, *25*, 514–517. [CrossRef]

24. Murai, M.; Okada, R.; Nishiyama, A.; Takai, K. Synthesis and properties of sila[*n*]helicenes via dehydrogenative silylation of C–H bonds under rhodium catalysis. *Org. Lett.* **2016**, *18*, 4380–4383. [CrossRef] [PubMed]

25. Tsurusaki, A.; Kobayashi, A.; Kyushin, S. Synthesis, structures, and electronic properties of dithienosiloles bearing bulky aryl groups: Conjugation between a π-electron system and "perpendicular" aryl groups. *Asian J. Org. Chem.* **2017**, *6*, 737–745. [CrossRef]

26. Maeda, H.; Suzuki, T.; Segi, M. Effects of substituents in silyl groups on the absorption, fluorescence and structural properties of 1,3,6,8-tetrasilylpyrenes. *Photochem. Photobiol. Sci.* **2018**, *17*, 781–792. [CrossRef]

27. Maeda, H.; Horikoshi, R.; Yamaji, M.; Furuyama, T.; Segi, M. Photophysical properties of silyl-substituted stilbene derivatives. *Eur. J. Org. Chem.* **2020**, *2020*, 3410–3422. [CrossRef]

28. Haruki, R.; Sasaki, Y.; Masutani, K.; Yanai, N.; Kimizuka, N. Leaping across the visible range: Near-infrared-to-violet photon upconversion employing silyl-substituted anthracene. *Chem. Commun.* **2020**, *56*, 7017–7020. [CrossRef]

29. Terada, N.; Uematsu, K.; Higuchi, R.; Tokimaru, Y.; Sato, Y.; Nakano, K.; Nozaki, K. Synthesis and properties of spiro-double sila[7]helicene: The LUMO spiro-conjugation. *Chem. Eur. J.* **2021**, *27*, 9342–9349. [CrossRef]

30. Benkyi, I.; Tapavicza, E.; Fliegl, H.; Sundholm, D. Calculation of vibrationally resolved absorption spectra of acenes and pyrene. *Phys. Chem. Chem. Phys.* **2019**, *21*, 21094–21103. [CrossRef]

31. Sambursky, S.; Wolfsohn, G. On the fluorescence and absorption spectra of anthracene and phenanthrene in solutions. *Trans. Faraday Soc.* **1940**, *35*, 427–432. [CrossRef]

32. Jones, N. The ultraviolet absorption spectra of anthracene derivatives. *Chem. Rev.* **1947**, *41*, 353–371. [CrossRef] [PubMed]

33. Schoof, S.; Güsten, H.; von Sonntag, C. Fluoreszenz und Fluoreszenzlöschung von meso-substituierten Anthracenderivaten in Lösung. *Ber. Bunsenges. Phys. Chem.* **1978**, *82*, 1068–1073. [CrossRef]

34. Hirayama, S.; Lampert, R.A.; Phillips, D. Photophysics of *meso*-substituted anthracenes. Part 1.—Solutions and isolated vapours. *J. Chem. Soc. Faraday Trans. 2* **1985**, *81*, 371–382. [CrossRef]

35. Klevens, H.B.; Platt, J.R. Spectral resemblances of cata-condensed hydrocarbons. *J. Chem. Phys.* **1949**, *17*, 470–481. [CrossRef]

36. Platt, J.R. Classification of spectra of cata-condensed hydrocarbons. *J. Chem. Phys.* **1949**, *17*, 484–495. [CrossRef]

37. Pariser, R. Theory of the electronic spectra and structure of the polyacenes and of alternant hydrocarbons. *J. Chem. Phys.* **1956**, *24*, 250–268. [CrossRef]

38. Heinrich, G.; Güsten, H. Deuterium-Isotopieeffekt auf die strahlende und strahlungslose Desaktivierung von Triplettzuständen polycyclischer aromatischer Kohlenwasserstoffe. *Z. Phys. Chem. (Wiesb.)* **1979**, *118*, 31–41. [CrossRef]

39. Brittain, E.F.H.; George, W.O.; Wells, C.H.J. *Introduction of Molecular Spectroscopy: Theory and Experiment*; Academic Press: London, UK; New York, NY, USA, 1970.

40. Orchin, M.; Jaffé, H.H. *Symmetry, Orbitals, and Spectra (S.O.S.)*; Wiley-Interscience: New York, NY, USA, 1971.

41. Klessinger, M.; Michl, J. *Excited States and Photochemistry of Organic Molecules*; VCH: New York, NY, USA, 1995.
42. Turro, N.J.; Ramamurthy, V.; Scaiano, J.C. *Modern Molecular Photochemistry of Organic Molecules*; University Science Books: Sausalito, CA, USA, 2010.
43. Franck, J.; Dymond, E.G. Elementary processes of photochemical reactions. *Trans. Faraday Soc.* **1926**, *21*, 536–542. [CrossRef]
44. Condon, E. A theory of intensity distribution in band systems. *Phys. Rev.* **1926**, *28*, 1182–1201. [CrossRef]
45. Frisch, M.J.; Trucks, G.W.; Schlegel, H.B.; Scuseria, G.E.; Robb, M.A.; Cheeseman, J.R.; Scalmani, G.; Barone, V.; Mennucci, B.; Petersson, G.A.; et al. *Gaussian 09*; Revision E.01; Gaussian, Inc.: Wallingford, CT, USA, 2013.
46. Frisch, M.J.; Trucks, G.W.; Schlegel, H.B.; Scuseria, G.E.; Robb, M.A.; Cheeseman, J.R.; Scalmani, G.; Barone, V.; Petersson, G.A.; Nakatsuji, H.; et al. *Gaussian 16*; Revision C.01; Gaussian, Inc.: Wallingford, CT, USA, 2019.